PERGAMON

Engineering Fracture Mechanics 69 (2002) 267–280

Engineering Fracture Mechanics

www.elsevier.com/locate/engfracmech

Fracture mechanics analysis of cracking in plain and reinforced concrete using the boundary element method

M.H. Aliabadi [a,*], A.L. Saleh [b]

[a] Department of Engineering, Queen Mary and Westfield College, University of London, Mile End Road, London E1 4NS, UK
[b] Faculty of Civil Engineering, Universiti Teknologi Malaysia, Johor Bahru, Malaysia

Abstract

Boundary element formulations for modelling the nonlinear behaviour of concrete are reviewed. The analysis based on the dual boundary element method (BEM) to represent the cracks in concrete is presented. The fictitious crack is adopted to represent the fracture process zone in concrete. The influence of reinforcements on the concrete is considered as a distribution of forces over the region of attachment. The yielding of reinforcement is considered when the total force at any section of the reinforcement is greater than the yielding force and is assumed to be broken when the strain reaches the maximum strain. In using the BEM to simulate cracks, the crack path need not be known in advance since it can be calculated during the iteration process and as such remeshing becomes obsolete. The numerical results obtained are compared to the FEM analysis.

Keywords: Fictitious crack model; Dual boundary element method; Boundary element method

1. Introduction

An early application of the boundary element method (BEM) to cracking can be traced to Harder [1]. An indirect boundary element formulation was used together with the fictitious crack model (FCM). No results were however reported in Ref. [1]. Liang and Li [2] presented BEM analysis to simulate the nonlinear fracture zone in cementatious materials, using a FCM. Later, Cen and Maier [3] used multidomain BEM along with the FCM to simulate the crack propagation in concrete. A review of boundary element formulations for fracture mechanics can be found in Ref. [4].

In this paper, the application of the BEM to analysis of crack growth in plain and reinforced concrete is presented. The method presented is based on the original contributions by Saleh and Aliabadi [8,10,11]. The FCM is used for the cracking of concrete and bonded by stiffener to represent the reinforcement. The method presented is based on the dual boundary element method (DBEM) developed by Aliabadi and co-workers [5–7]. The DBEM is shown to be computationally efficient in simulating crack propagation, particularly when dealing with the nonlinear behaviour in concrete such as fracture zone. Using this

* Corresponding author. Tel.: +44-020-7882-5301; fax: +44-020-983-1007.
E-mail address: m.h.aliabadi@qmw.ac.uk (M.H. Aliabadi).

0013-7944/02/$ - see front matter
PII: S0013-7944(01)00089-3

method the crack propagation path does not need to be known in advance, since at every step of crack extension the path is computed simultaneously. This is one of the main reasons why DBEM becomes more efficient in the numerical analysis of crack propagation in which the crack path could be arbitrary.

Therefore, the aim of this paper is to discuss the application of DBEM to the analysis of cracks in concrete and to study the behaviour of the fracture zone which occurred in concrete during the crack propagation, by means of the FCM.

2. Dual boundary element method

The DBEM is employed to model the cracking of reinforced concrete. The DBEM is shown to be computationally efficient in simulating crack propagation especially when dealing with the nonlinear behaviour in concrete. The dual equations, on which the DBEM is based, are the displacement and the traction boundary integral equations. The boundary integral representation of the displacement components, u_j can be written in terms of boundary points as

$$c_{ij}(\mathbf{x}')u_j(\mathbf{x}') + \oint_{\Gamma-\Gamma_{cr}} T_{ij}(\mathbf{x}',\mathbf{x})u_j(\mathbf{x})\,d\Gamma(\mathbf{x}) + \oint_{\Gamma_{cr}} T_{ij}(\mathbf{x}',\mathbf{x})u_j^{cr}(\mathbf{x})\,d\Gamma_{cr}(\mathbf{x}) - \int_{\Gamma_{cr}} U_{ij}(\mathbf{x}',\mathbf{x})t_j^{cr}(\mathbf{x})\,d\Gamma_{cr}(\mathbf{x}) = \int_{\Gamma-\Gamma_{cr}} U_{ij}(\mathbf{x}',\mathbf{x})t_j(\mathbf{x})\,d\Gamma(\mathbf{x}), \tag{1}$$

where coefficient $c_{ij}(\mathbf{x}')$ is given by $\delta_{ij}/2$ for smooth boundary at the point $\mathbf{x}'$ (δ_{ij} is the Kronecker delta) and $\oint$ denote the Cauchy principal value integral. The functions $T_{ij}(\mathbf{x}',\mathbf{x})$ and $U_{ij}(\mathbf{x}',\mathbf{x})$ represent the Kelvin traction and displacement fundamental solutions, given by

$$U_{ij}(\mathbf{x}',\mathbf{x}) = -\frac{1+v}{4\pi(1-v)E}\{(3-4v)\ln(r)\delta_{ij} - r_{,i}r_{,j}\},$$

$$T_{ij}(\mathbf{x}',\mathbf{x}) = -\frac{1}{4\pi(1-v)r}\left\{[(1-2v)\delta_{ij} + 2r_{,i}r_{,j}]\frac{\partial r}{\partial n} - (1-2v)(r_{,i}n_j - r_{,j}n_i)\right\}.$$

At a boundary point $\mathbf{x}$; $u_j^{cr}(\mathbf{x})$ and $t_j^{cr}(\mathbf{x})$ are the displacement and distributed cohesive forces, respectively, on one of the crack surfaces, Γ_{cr}.

The boundary integral representation of the traction components, t_j can be obtained from $t_j = \sigma_{ij}n_i$, where σ_{ij} are the stress components obtained by differentiating Eq. (1) followed by application of the Hooke's law and n_i denotes the ith component of the unit outward normal to the boundary. For a point on a smooth boundary, t_j can be written as

$$\frac{1}{2}t_j(\mathbf{x}') + n_i(\mathbf{x}')\oint\!\!\!\!\!\!=_{\Gamma-\Gamma_{cr}} S_{kij}(\mathbf{x}',\mathbf{x})u_k(\mathbf{x})\,d\Gamma(\mathbf{x}) + n_i(\mathbf{x}')\oint\!\!\!\!\!\!=_{\Gamma_{cr}} S_{kij}(\mathbf{x}',\mathbf{x})u_k^{cr}(\mathbf{x})\,d\Gamma_{cr}(\mathbf{x}) - n_i(\mathbf{x}')\oint_{\Gamma_{cr}} D_{kij}(\mathbf{x}',\mathbf{x})t_k^{cr}(\mathbf{x})\,d\Gamma_{cr}(\mathbf{x}) = n_i(\mathbf{x}')\oint_{\Gamma-\Gamma_{cr}} D_{kij}(\mathbf{x}',\mathbf{x})t_k(x)\,d\Gamma(\mathbf{x}), \tag{2}$$

where $\oint\!\!\!\!\!\!=$ denotes the Hadamard principal value integral. The fundamental solutions $S_{kij}(\mathbf{x}',\mathbf{x})$ and $D_{kij}(\mathbf{x}',\mathbf{x})$ are given as

$$S_{kij}(\mathbf{x}',\mathbf{x}) = \frac{E}{4\pi(1-v^2)r^2}\left\{2\frac{\partial r}{\partial n}[(1-2v)\delta_{ij}r_{,k} + v(\delta_{ik}r_{,j} + \delta_{jk}r_{,i}) - 4r_{,i}r_{,j}r_{,k}] + 2v(n_ir_{,j}r_{,k} + n_jr_{,k}r_{,i}) + (1-2v)(2n_kr_{,i}r_{,j} + n_j\delta_{ik} + n_i\delta_{jk}) - (1-4v)n_k\delta_{ij}\right\}$$

and

$$D_{kij}(\mathbf{x}',\mathbf{x}) = \frac{1}{4\pi(1-\nu)r}\left\{(1-2\nu)(\delta_{kj}r_{,j} + \delta_{kj}r_{,i} - \delta_{ij}r_{,k}) + 2r_{,i}r_{,j}r_{,k}\right\}.$$

The functions $u_k^{\mathrm{cr}}(\mathbf{x})$ and $t_k^{\mathrm{cr}}(\mathbf{x})$ are the displacement and distributed cohesive forces, respectively, at the other crack surfaces, Γ_{cr}. For a traction free crack, $t_j^{\mathrm{cr}} = t_k^{\mathrm{cr}} = 0$. Eqs. (1) and (2) constitute the basis of the DBEM and can be expressed in the matrix form as

$$[A \quad [H_{\mathrm{cr}}] \quad [G_{\mathrm{cr}}]] \begin{Bmatrix} X \\ \{u_{\mathrm{cr}}\} \\ \{t_{\mathrm{cr}}\} \end{Bmatrix} = \{F\}, \tag{3}$$

in which A is the coefficient corresponding to vector X containing the unknowns u and t and F contains the known values of u and t on the boundary nodes other than the crack boundary. $[H_{\mathrm{cr}}]$ and $[G_{\mathrm{cr}}]$ are coefficients corresponding to the nodes on the crack boundary. The general modelling strategy developed by Portela et al. [6] is adopted in this work.

The general modelling strategy is as follows:

- for the crack boundary, the displacement boundary integral equation is applied when the source point is located on one of the crack surfaces;
- the traction boundary integral equation is applied when the source point is located on the opposite crack boundary;
- the displacement boundary integral equation is applied when the source point is located on the remaining noncracked boundaries of the body;
- the crack boundaries are discretized by discontinuous quadratic boundary elements. The nodes of one of the crack boundaries are located in such a way that they coincide with the nodes on the opposite boundary;
- continuous quadratic boundary elements are used along the remaining noncrack boundaries of the body, except at the intersection between a crack and an edge, where discontinuous quadratic elements are used in order to avoid nodes at the intersection.

3. Boundary condition for FCM

The cohesive forces on the fictitious crack surfaces, i.e. the fracture zone, can be derived by the relationship between traction and crack opening displacement in the local coordinate system (n,t). The linear (SL) softening constitutive law, can be written as

$$t_n^{\mathrm{cr}} = f_t'\left(-\frac{\Delta u_n^{\mathrm{cr}}}{\Delta u_c^{\mathrm{cr}}}\right), \quad t_{nt}^{\mathrm{cr}} = 0, \tag{4}$$

where $\Delta u_n^{\mathrm{cr}} = u_n^b - u_n^a$ is a displacement discontinuity normal to the crack in which u_n^a is the displacement at one of the crack surfaces and u_n^b is the displacement at the opposite crack surface. Δu_c^{cr} and f_t' are the material parameters. At the interface of the fracture zone, to maintain the equilibrium, the following conditions are enforced

$$u_n^a = u_n^b, \quad t_n^a = -t_n^b, \quad t_t^a = -t_t^b. \tag{5}$$

The combination of boundary integral equation, Eqs. (1) and (2), and the fictitious crack boundary condition, Eqs. (3) and (4), can be expressed in the matrix form as

$$\begin{bmatrix} A & [H_{cr}] & [G_{cr}] \\ 0 & [C_{cr}] & [D_{cr}] \end{bmatrix} \begin{Bmatrix} X \\ \{u_{cr}\} \\ \{t_{cr}\} \end{Bmatrix} = \begin{Bmatrix} F \\ \{S_{cr}\} \end{Bmatrix}, \tag{6}$$

where $[C_{cr}]$ and $[D_{cr}]$ are the fictitious crack boundary conditions corresponding to the vectors $\{u_{cr}\}$ and $\{t_{cr}\}$, respectively, and the vector $\{S_{cr}\}$ contains the material parameters. In all cases, subscript cr represents the fictitious crack boundary. For the linear relation $\sigma - \Delta u_n^{cr}$, matrices $[C_{cr}]$ and $[D_{cr}]$ contain 4×4 submatrices given by

$$[C_{cr}] = \begin{bmatrix} -\frac{f_t'}{\Delta u_c^{cr}} & 0 & \frac{f_t'}{\Delta u_c^{cr}} & 0 \\ 0 & -1 & 0 & 1 \\ 0 & 0 & 0 & 0 \\ 0 & 0 & 0 & 0 \end{bmatrix}, \qquad [D_{cr}] = \begin{bmatrix} 1 & 0 & 0 & 0 \\ 0 & 0 & 0 & 0 \\ 1 & 0 & 1 & 0 \\ 0 & 1 & 0 & 1 \end{bmatrix}, \tag{7}$$

and vectors $\{u_{cr}\}$, $\{t_{cr}\}$ and $\{S_{cr}\}$ are given by

$$\{u_{cr}\} = [N] \begin{Bmatrix} u_x^a \\ u_y^a \\ u_x^b \\ u_y^b \end{Bmatrix}, \qquad \{t_{cr}\} = [N] \begin{Bmatrix} t_x^a \\ t_y^a \\ t_x^b \\ t_y^b \end{Bmatrix}, \qquad \{S_{cr}\} = \begin{Bmatrix} f_t' \\ 0 \\ 0 \\ 0 \end{Bmatrix}, \tag{8}$$

where $[N]$ is the transformation matrix from global to the local reference system, varying node by node on the fictitious crack surface.

The cracked boundaries are modelled with discontinuous quadratic elements (see Fig. 2). This is due to the efficiency and to keep the simplicity of the standard boundary elements. Continuous quadratic elements are used along the remaining boundary of the body, except at the intersection between a crack and an edge, where discontinuous elements are required on the edge in order to avoid a common node at the intersection.

4. Modelling of reinforcements

Consider the cracked reinforced concrete configuration shown in Fig. 1(a). In addition to the plain concrete, a number of reinforcements are bonded to the concrete over the loci L_n $(n = 1, 2, \ldots, N^{st})$, where N^{st} is the number of reinforcements.

The reinforcement is subdivided into continuous quadratic isoparametric elements which consist of three nodes equally spaced by, b_n. Each reinforcement exerts a line distribution of forces (per unit arc length), $f_j^n(\mathbf{X})$ $(j = 1, 2;\ n = 1, 2, \ldots, N^{st})$ on the corresponding locus L_n in the concrete, and itself experiences an equal and opposite reaction force $-f_j^n(\mathbf{X})$ along its length. The condition that the concrete displacements $u_j(\mathbf{X})$ and the nth reinforcement displacements $u_j^n(\mathbf{X})$ are compatible with the shear coefficient of the bond between concrete and reinforcement, Φ^n, is given in terms of f_j^n by

$$\left[u_j^n(\mathbf{X}') - u_j^n(\mathbf{X}_0)\right] - \left[u_j(\mathbf{X}') - u_j(\mathbf{X}_0)\right] = \Phi^n \left[f_j^n(\mathbf{X}') - f_j^n(\mathbf{X}_0)\right], \tag{9}$$

where $\mathbf{X}_0$ and $\mathbf{X}'$ are distinct points on the nth reinforcement locus L_n. For a perfect bond, Φ^n is equal to zero.

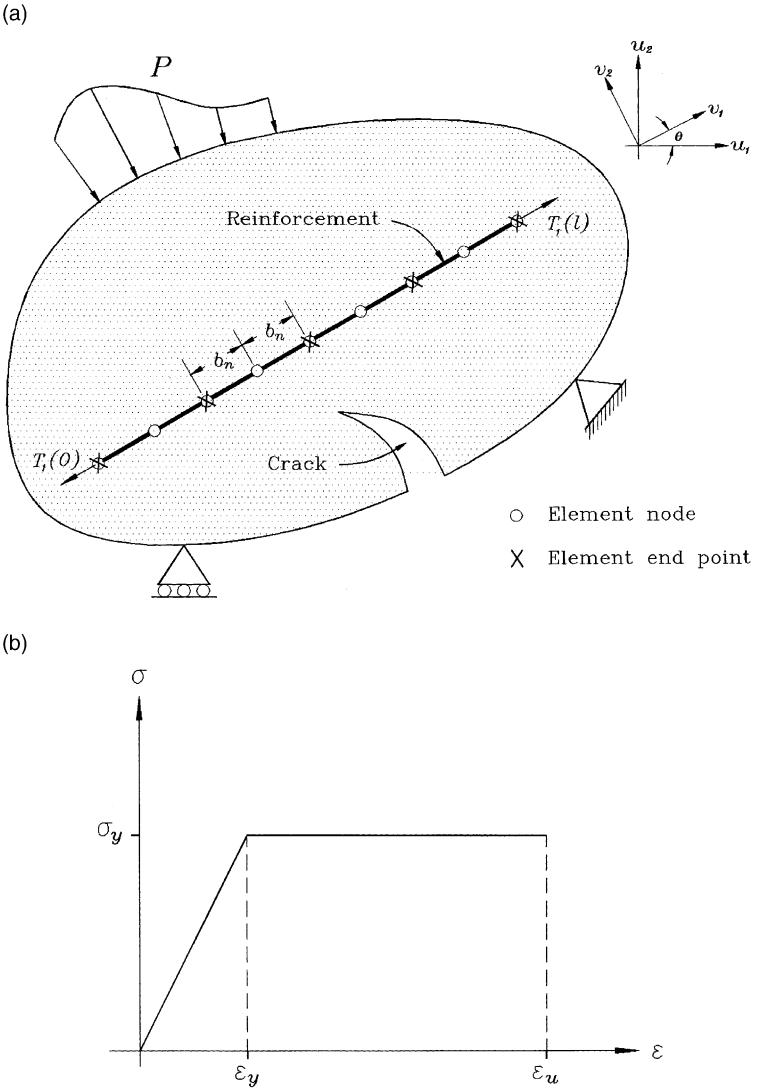

Fig. 1. Reinforced concrete configuration: (a) Steel nodes are divided into equal intervals. (b) The stress–strain curve for steel is assumed to be elastic perfectly plastic.

The reaction forces of the reinforcement, $f_j^n(\mathbf{X})$, can be included in the displacement boundary integral equation (1) as the body forces confined to a straight line instead of to the domain and are given by

$$c_{ij}(\mathbf{x}')u_j(\mathbf{x}') + \oint_{\Gamma-\Gamma_{\rm cr}} T_{ij}(\mathbf{x}',\mathbf{x})u_j(\mathbf{x})\,\mathrm{d}\Gamma(\mathbf{x}) + \oint_{\Gamma_{\rm cr}} T_{ij}(\mathbf{x}',\mathbf{x})u_j^{\rm cr}(\mathbf{x})\,\mathrm{d}\Gamma_{\rm cr}(\mathbf{x}) - \int_{\Gamma_{\rm cr}} U_{ij}(\mathbf{x}',\mathbf{x})t_j^{\rm cr}(\mathbf{x})\,\mathrm{d}\Gamma_{\rm cr}(\mathbf{x})$$
$$- \sum_{n=1}^{N^{\rm st}} \int_{L_n} U_{ij}(\mathbf{x}',\mathbf{X})f_j^n(\mathbf{X})\,\mathrm{d}L_n(\mathbf{X}) = \int_{\Gamma-\Gamma_{\rm cr}} U_{ij}(\mathbf{x}',\mathbf{x})t_j(\mathbf{x})\,\mathrm{d}\Gamma(\mathbf{x}), \tag{10}$$

and in the traction boundary integral equation (2), as

$$\frac{1}{2}t_j(\mathbf{x}') + n_i(\mathbf{x}')\oint_{\Gamma-\Gamma_{cr}} S_{kij}(\mathbf{x}',\mathbf{x})u_k(\mathbf{x})\,d\Gamma(\mathbf{x}) + n_i(\mathbf{x}')\oint_{\Gamma_{cr}} S_{kij}(\mathbf{x}',\mathbf{x})u_k^{cr}(\mathbf{x})\,d\Gamma_{cr}(\mathbf{x})$$
$$- n_i(\mathbf{x}')\int_{\Gamma_{cr}} D_{kij}(\mathbf{x}',\mathbf{x})t_k^{cr}(\mathbf{x})\,d\Gamma_{cr}(\mathbf{x}) - n_i(\mathbf{x}')\sum_{n=1}^{N^{st}}\int_{L_n} D_{ijk}(\mathbf{x}',\mathbf{X})f_k^n(\mathbf{X})\,dL_n(\mathbf{X})$$
$$= n_i(\mathbf{x}')\oint_{\Gamma-\Gamma_{cr}} D_{kij}(\mathbf{x}',\mathbf{x})t_k(x)\,d\Gamma(\mathbf{x}). \tag{11}$$

Combining Eq. (9) with Eqs. (10) and (11) gives the compatibility equation for points $\mathbf{X}_0$ and $\mathbf{X}'$ on the nth reinforcement locus as

$$\left[u_j^n(\mathbf{X}') - u_j^n(\mathbf{X}_0)\right] + \oint_{\Gamma-\Gamma_{cr}} \Delta T_{ij}u_j(\mathbf{x})\,d\Gamma(\mathbf{x}) + \oint_{\Gamma-\Gamma_{cr}} \Delta T_{ij}u_j^{cr}(\mathbf{x})\,d\Gamma_{cr}(\mathbf{x}) - \int_{\Gamma_{cr}} \Delta U_{ij}t_j^{cr}(\mathbf{x})\,d\Gamma_{cr}(\mathbf{x})$$
$$- n_i(\mathbf{X})\oint_{\Gamma} \Delta S_{kij}u_k(\mathbf{x})\,d\Gamma(\mathbf{x}) - n_i(\mathbf{X})\int_{\Gamma_{cr}} \Delta D_{kij}t_k^{cr}(\mathbf{x})\,d\Gamma_{cr}(\mathbf{x}) - \sum_{n=1}^{N^{st}}\int_{L_n} U_{ij}(\mathbf{X}'-\mathbf{X}_0)f_j^n(\mathbf{X})\,dL_n(\mathbf{X})$$
$$= \int_{\Gamma-\Gamma_{cr}} \Delta U_{ij}t_j(\mathbf{x})\,d\Gamma(\mathbf{x}) + n_i(\mathbf{X})\int_{\Gamma-\Gamma_{cr}} \Delta D_{kij}t_k(\mathbf{x})\,d\Gamma(\mathbf{x}), \tag{12}$$

where $\Phi^n = 0$ is assumed and,

$$\begin{aligned}
\Delta T_{ij} &= T_{ij}(\mathbf{X}',\mathbf{x}) - T_{ij}(\mathbf{X}_0,\mathbf{x}),\\
\Delta U_{ij} &= U_{ij}(\mathbf{X}',\mathbf{x}) - U_{ij}(\mathbf{X}_0,\mathbf{x}),\\
\Delta S_{kij} &= S_{kij}(\mathbf{X}',\mathbf{x}) - S_{kij}(\mathbf{X}_0,\mathbf{x}),\\
\Delta D_{kij} &= D_{kij}(\mathbf{X}',\mathbf{x}) - D_{kij}(\mathbf{X}_0,\mathbf{x}).
\end{aligned} \tag{13}$$

The displacements u_j^n of the nth reinforcement in Eq. (12) can be expressed in terms of an arc length parameter x measured in the longitudinal direction from one end. Therefore, the relative displacements of the reinforcement due to a body force distribution $-f_j(x)$ per unit length $(0 < x \leqslant l)$ are given by

$$u_j(x) - u_j(0) = [N]\left[v_j(x) - v_j(0)\right] \quad \text{for } j = 1,2, \tag{14}$$

where $[N]$ represents the transformation matrix from global to local coordinate system. The displacements v_j of the reinforcement along the longitudinal direction are given as

$$[v_1(x) - v_1(0)] = \frac{1}{A_s E_s}\left\{xT_1(0) + \int_0^x (x-\xi)f_1(\xi)\,d\xi\right\} \tag{15}$$

and along the transverse direction as

$$[v_2(x) - v_2(0)] = \frac{1}{A_s G_s}\left\{xT_2(0) + \int_0^x (x-\xi)f_2(\xi)\,d\xi\right\}$$
$$- \frac{1}{R_s}\left\{\frac{1}{2}x^2M(0) + \frac{1}{6}x^3T_2(0) + \int_0^x \frac{1}{6}(x-\xi)^3 f_2(\xi)\,d\xi\right\} - x\beta(0), \tag{16}$$

where A_s, E_s, G_s and R_s are material properties and represent the cross-sectional area, Young's modulus, shear modulus and transverse flexural rigidity of the reinforcement; $T_1(x)$, $T_2(x)$ and $M(x)$ representing the internal forces and moment acting over the reinforcement cross-section and $\beta(0)$ denoting the partial derivative $\partial v_1/\partial y$ evaluated at the end $x = 0$ to take account of any difference in the rigid body rotations of reinforcement and concrete.

Additional equations are those of equilibrium under the actions of the body forces $-f_j(x)$ and the end loads $T_1(0)$, $T_1(l)$, $T_2(0)$, $T_2(l)$, and $M(0)$, $M(l)$. They can be expressed as

$$\begin{aligned} &\int_0^l f_j(x)\,\mathrm{d}x = T_j(l) - T_j(0) \quad \text{for } j = 1,2, \\ &\int_0^l (l-x) f_2(x)\,\mathrm{d}x = M(l) - M(0) - lT_2(0). \end{aligned} \tag{17}$$

The end loads in Eq. (17) correspond to the boundary conditions for the reinforcement. Setting all six values to zero will represent a reinforcement with free ends. Alternatively, finite values may be chosen to specify a given state of stress or strain at the ends.

5. Yielding of reinforcement

The reinforcements are assumed to behave linearly up to the yield stress, σ_Y, and then as a perfectly plastic material as shown in the stress–strain curve in Fig. 1(b). After yielding, the force in the reinforcement is set to the yielding force, $F_y = \sigma_Y A_s$ until the strain reaches the maximum strain, ε_{su}, when the reinforcement is broken. The total force at any node in the reinforcement, F_n, is determined from the end load $T_1(0)$ and the summation of forces (per unit arc length), f_j, multiplied by the node interval, b_n as

$$F_n = T_1(0) + b_n \sum_{j=n}^{N} f_j. \tag{18}$$

The total force in Eq. (19) is compared with the yielding force, F_y. If the force is greater than the yielding force, all the affected nodes ($j = n, \ldots, N$) are set to a value in such a way that the summation of forces per unit arc length at that particular node is equal to the yielding force per unit length, F_y/b_n.

6. Algorithm for crack growth

The direction of propagation of the fictitious crack is obtained from maximum principal stress criteria as given by

$$\phi = \frac{1}{2}\tan^{-1}\left[\frac{2\tau_{xy}}{\sigma_x - \sigma_y}\right]. \tag{19}$$

With reference to Fig. 2, the iteration process can be described by the following:

(1) The initial load $\mathbf{P}^1_{\text{init}}$ is given to calculate the stress components $(\sigma^1_n, \sigma^1_t, \tau^1_{nt})$ at the initial crack tip.

(2) An increase in the load by a certain amount, say λ, such that $\mathbf{P}^2_{\text{init}} = \mathbf{P}^1_{\text{init}} + \lambda$, and calculating the stress components $(\sigma^1_n, \sigma^1_t, \tau^1_{nt})$ at the initial crack tip (in the current step). In this step, it is possible to determine the characteristics of the final load, $\mathbf{P}^3_{\text{init}}$ whether in the ascending branch when $S_\theta < 0$ or in the descending branch when $S_\theta > 0$ where,

$$S_\theta = \frac{\mathbf{P}^1_{\text{init}} - \mathbf{P}^2_{\text{init}}}{\sigma^1_n - \sigma^2_n}. \tag{20}$$

(3) Once the characteristic of the final load has been calculated, $\mathbf{P}^3_{\text{init}}$ can be calculated using linear extrapolation of the load and the normal stress, $(\mathbf{P}^1_{\text{init}}, \sigma^1_n)$ and $(\mathbf{P}^2_{\text{init}}, \sigma^2_n)$ using the following expression:

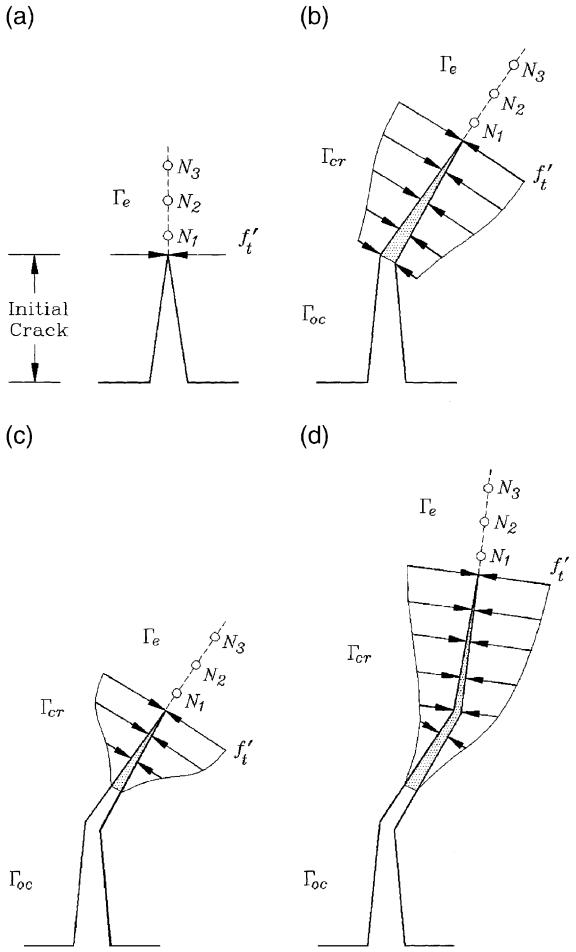

Fig. 2. Schematic illustration of the iteration process: Calculation of stresses for (a) the initial crack tip, (b) the first increment, (c) some elements at the fictitious crack tip will be completely separated when $\Delta u^{\mathrm{cr}} > \Delta u_c$ and (d) increment of the next element. Γ_{oc}, Γ_{cr} and Γ_{e} represent the open crack boundary, fictitious crack boundary and elastic boundary, respectively.

$$\begin{aligned}
\mathbf{P}^3_{\mathrm{init}} &= \mathbf{P}^1_{\mathrm{init}} + \left[(f_t' - \sigma_n^1)\frac{\mathbf{P}^1_{\mathrm{init}} - \mathbf{P}^2_{\mathrm{init}}}{\sigma_n^1 - \sigma_n^2}\right], \quad \text{for } \sigma_n^2 > f_t' \\
\mathbf{P}^3_{\mathrm{init}} &= \mathbf{P}^1_{\mathrm{init}} + \left[(f_t' - \sigma_n^2)\frac{\mathbf{P}^1_{\mathrm{init}} - \mathbf{P}^2_{\mathrm{init}}}{\sigma_n^1 - \sigma_n^2}\right], \quad \text{for } \sigma_n^2 < f_t'
\end{aligned} \tag{21}$$

for $S_\theta < 0$ and

$$\begin{aligned}
\mathbf{P}^3_{\mathrm{init}} &= \mathbf{P}^1_{\mathrm{init}} - \left[(f_t' - \sigma_n^1)\frac{\mathbf{P}^1_{\mathrm{init}} - \mathbf{P}^2_{\mathrm{init}}}{\sigma_n^1 - \sigma_n^2}\right], \quad \text{for } \sigma_n^2 > f_t' \\
\mathbf{P}^3_{\mathrm{init}} &= \mathbf{P}^1_{\mathrm{init}} - \left[(f_t' - \sigma_n^2)\frac{\mathbf{P}^1_{\mathrm{init}} - \mathbf{P}^2_{\mathrm{init}}}{\sigma_n^1 - \sigma_n^2}\right], \quad \text{for } \sigma_n^2 < f_t'
\end{aligned} \tag{22}$$

for $S_\theta > 0$. Again, calculate the stress components at the initial crack tip, and now the normal stress is equal to the maximum tensile strength of the material, i.e. $\sigma_n^3 = f_t'$ (see Fig. 2(a)). Having obtained the final stress components, it is possible to calculate the direction of the crack propagation, ϕ_{init}, using Eq. (19). This is the final step for the first iteration and therefore, $\mathbf{P}_{\text{init}}^3$ becomes the final load for this iteration.

(4) An increase in the crack length by a specified amount in the direction perpendicular to ϕ_{init}. Repeat steps (1–3) to obtain the final load for this increment, $\mathbf{P}_{\text{init}}^3$ becomes the direction, ϕ_m (see Fig. 2(b)).

(5) Check the normal crack opening displacement, Δu_n^{cr}, at the real crack tip. In the case when Δu_n^{cr} is greater than the critical value, Δu_c, the real crack tip moves to the adjacent element and the fictitious crack will completely separate and become a traction free crack (see Fig. 2(c)). In this case the system of linear algebraic equations will be changed. Repeat steps (1–3) again to calculate the new final load and the path.

(6) If step (5) does not apply, the crack will propagate perpendicular to ϕ_m with a specified crack length extension.

(7) Repeat steps (1–6) for the next crack extension (Fig. 2(d)).

Using the above iteration procedure, the final load for each crack extension can be approximately calculated and the crack path does not have to be known in advance. The path can be in any direction and its true as long as the above procedure is preserved. This is perhaps one of the advantages of using DBEM in crack growth analysis over the other methods.

7. Numerical example

In this section examples of crack growth in plain and reinforced concrete are presented. Also presented are comparisons with the finite element method.

7.1. Double notched problem

Consider a double notched shear beam shown in Fig. 3. The geometrical ratios considered in this example are $l/h = 4.0$, $c/h = 0.8$, $a/h = 0.2$ and $b/h = 1.0$, where b is the thickness of the beam. The depth of the beam is $h = 0.2$ m. This beam has been analyzed using FEM by Carpinteri [12]. A similar beam with different ratios has also been tested by many other researchers. The concrete has been modelled as linearly elastic with compression $E_c = 27\,000$ MPa and $v = 0.1$. The mode I crack parameters have been taken as tensile strength, $f_t' = 2.0$ MPa and fracture energy, $G_f = 100$ N/m. The structure has symmetry about two axes, i.e. the horizontal and vertical axes at the centre of the beam. This symmetry will make the structure balance and have a polar symmetry around the centre. The initial boundary element mesh contains 98 nodes with 44 elements.

The initial boundary element mesh is shown in Fig. 4 followed by the deformation shape at a certain iteration. The history of the crack pattern is shown in Fig. 5. Fig. 6, shows the dimensionless computational results in terms of load–deflection curves for the bending point C of steel beam.

7.2. Reinforced concrete beam

Consider the beam shown in Fig. 7. The material properties for the concrete are as follows: compression strength $f_c = 75.5$ MPa, Young's modulus $E_c = 34\,300$ MPa, fracture energy $G_f = 90$ N/m, tensile strength $f_t' = 5.30$ MPa. The beam of $h = 100$ mm with an area of steel $A_s = 157.1$ mm^2 is considered. The diameter of the hole is 30 mm. In the first case, a hole is introduced 50 mm away from the centre line of the beam. In the second case, two symmetrical holes are introduced. In the third case, the hole is placed in an area where

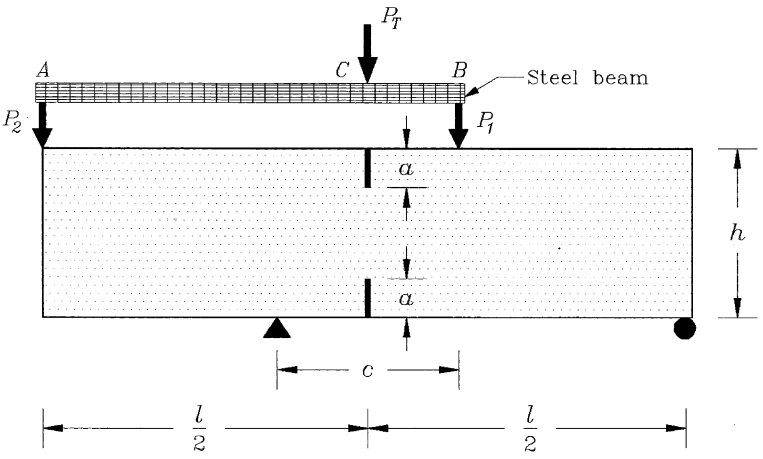

Fig. 3. Double notched shear beam for mixed mode crack propagation.

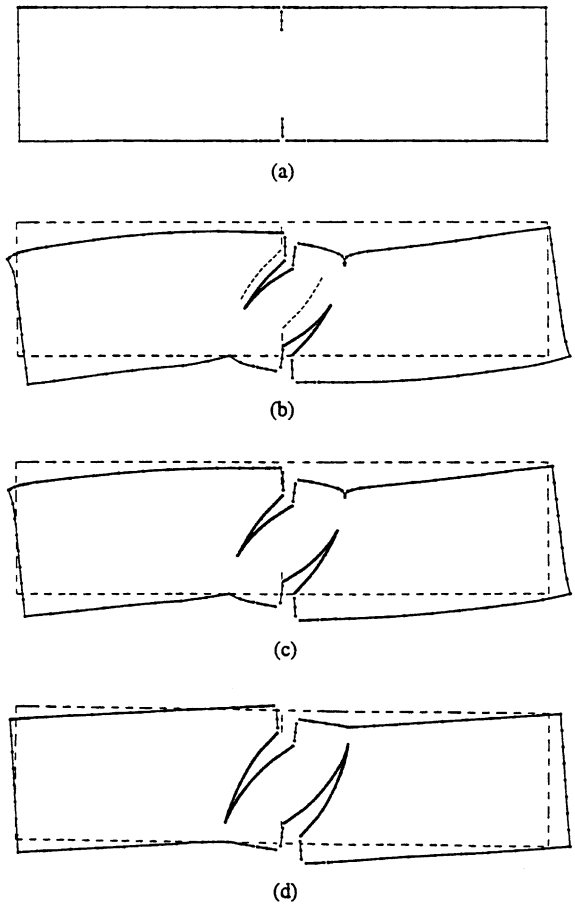

Fig. 4. (a) Initial boundary element mesh and deformation shape for (b) iteration 3, (c) iteration 6 and (d) iteration 8.

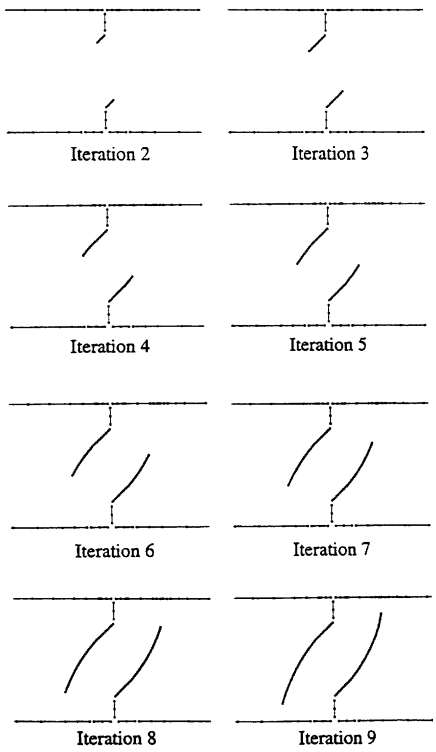

Fig. 5. The history of the crack path for a double notched shear beam.

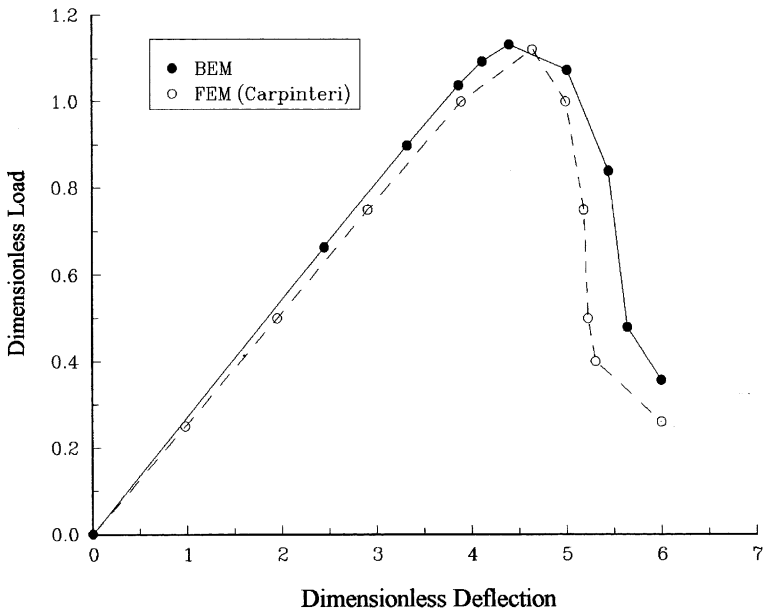

Fig. 6. Total load against deflection at point C of a double notched shear beam.

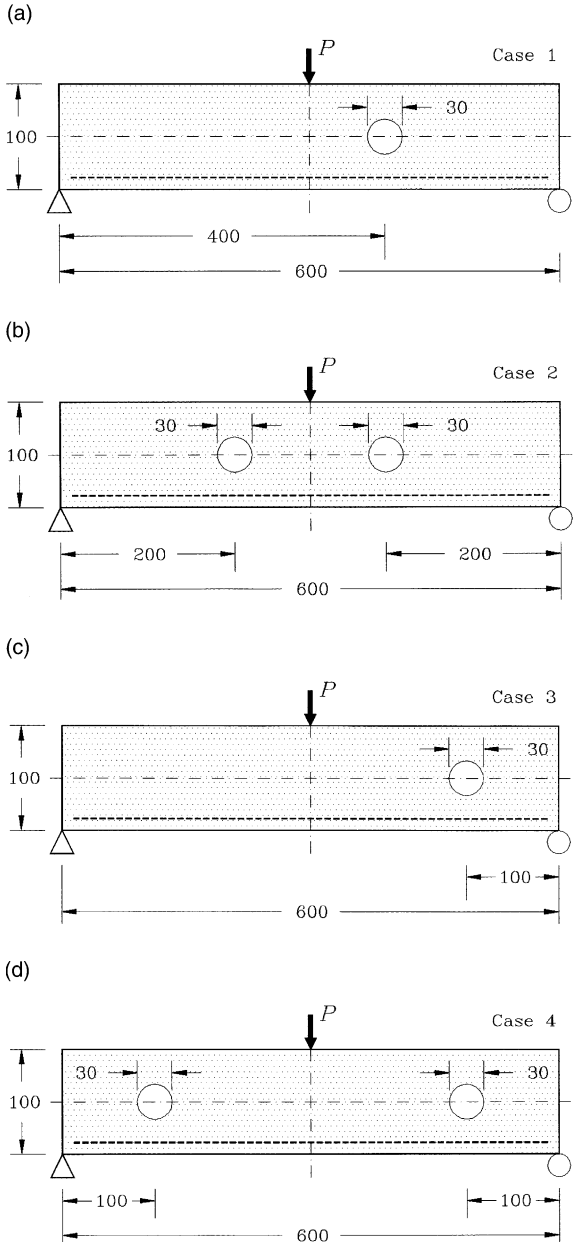

Fig. 7. Three-point bending beam with the presentation of holes.

the diagonal tension crack is to appear. The fourth case is similar to the third case, except that there are two holes located in the area of the diagonal tension crack.

The results for these analyses are shown in Fig. 8. From the figure, it can be observed that there are no extreme changes in terms of load carrying capacity for all cases. Very minor changes can be seen for the mid-span deflection.

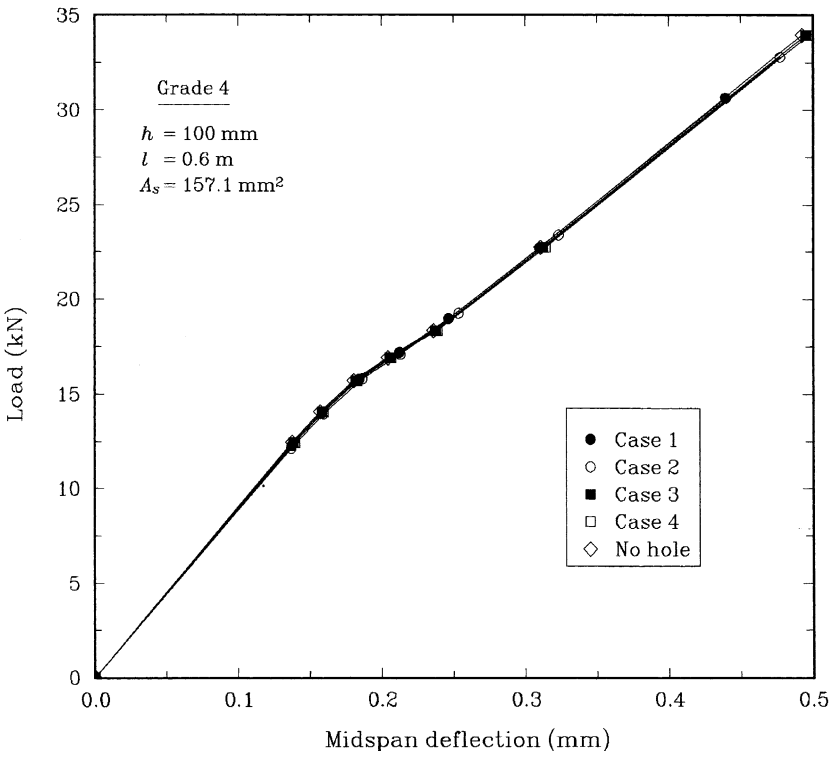

Fig. 8. Load–deflection curves for concrete grade four with the presentation of holes.

8. Conclusion

A boundary element formulation has been presented for modelling cracking in plain and reinforced concrete. The model utilized the fictitious crack model for the cracking of concrete. Both the linear and bilinear stress-displacement curve have been implemented. The BEM results were shown to agree well with the FEM. The advantage of the new formulation over previous ones was demonstrated by simulating crack growth where no remeshing is required.

The embedded approach is used to model the reinforcement. The proposed model has a capability to detect the yield stress in the steel with reasonable accuracy. It is assumed that the bond between steel and concrete is perfect.

References

[1] Harder NA. Computer simulated crack propagation in concrete beams by means of the fictitious crack method and the boundary element method. 2nd ed. Department of Building Technology and Structural Engineering, University of Aalborg, Denmark, ISSN 0902–7513 R8822, 1991.

[2] Liang RYK, Li Y-N. Simulations of nonlinear fracture process zone in cementatious material—a boundary element approach. Computat Mech 1991;7:413–27.

[3] Cen Z, Maier G. Bifurcations and instabilities in fracture of cohesive-softening structures: a boundary element analysis. Fatigue Fract Eng Mater Struct 1992;15:911–28.

[4] Aliabadi MH. Boundary element formulations in fracture mechanics. Appl Mech Rev 1997;50:83–96.

[5] Aliabadi MH. A new generation of boundary element methods in fracture mechanics. Int J Fract 1997;86:91–125.
[6] Portela A, Aliabadi MH, Rooke DP. Dual boundary element method for pin-loaded lugs. Bound Elem Tech 1991;VI:381–92.
[7] Mi Y, Aliabadi MH. Dual boundary element method for analysis for three-dimensional fracture mechanics analysis. Eng Anal 1992;10:161–71.
[8] Saleh AL, Aliabadi MH. Crack growth analysis in concrete using boundary element method. Eng Fract Mech 1995;51(4):533–45.
[10] Saleh AL, Aliabadi MH. Crack growth analysis in reinforced concrete using the boundary element method. J Mech ASCE. 1998.
[11] Saleh AL, Aliabadi MH. Boundary element analysis of the pull-out behaviour of an anchor bolt embedded in concrete. Mech Cohes-Frict Mater 1996;1:235–50.
[12] Carpinteri A. Post-peak and post-bifurcation analysis of cohesive crack propagation. Eng Fract Mech 1989;32:265–78.